frontiers in Materials

ORIGINAL RESEARCH
published: 15 February 2022
doi: 10.3389/fmats.2022.822589

Effect of Al_3Zr Dispersoid on Microstructure and Mechanical Properties of Al-Cu-Li Alloy During Composite Spinning-Extrusion Forming

Jin Zhang[1,2], *Huaqiang Zeng*[1], *Cheng Wang*[1]* *and Zibo Tang*[1]

[1]Light Alloy Research Institute, Central South University, Changsha, China, [2]State Key Laboratory of High Performance and Complex Manufacturing, Central South University, Changsha, China

The regulation of blank microstructure is the key to manufacturing high-quality ring cylinder by composite spinning - extrusion forming. In this paper, the precipitation morphologies of three Al_3Zr dispersions were obtained by changing the heat treatment process, and their effects on the microstructure and mechanical properties of Al-Cu-Li alloy ring cylinder were investigated. The results show that the microstructure and mechanical properties of ring cylinder are affected by the different precipitation distribution of Al_3Zr dispersoids in the blank. When the Al_3Zr dispersoids precipitated and dispersed, the cracking of ring cylinder was eliminated, the thickness of coarse-grained layer decreases obviously, and the elongation is increased by 33.5%. In the T83 state, the average length of the T_1 phase decreased from 100.3 to 77.5 nm, while the tensile strength and yield strength of ring cylinder increased by 16 and 20 MPa, respectively.

Keywords: Al-Cu-Li alloy, composite spinning-extrusion forming, Al3Zr dispersoids, microstructure, mechanical properties

OPEN ACCESS

Edited by:
Peng Cao,
The University of Auckland, New Zealand

Reviewed by:
Changjiang Zhang,
Taiyuan University of Technology, China
Sudagar J.,
VIT-AP University, India

***Correspondence:**
Cheng Wang
peterchenglari@csu.edu.cn

Specialty section:
This article was submitted to Structural Materials, a section of the journal Frontiers in Materials

Received: *26 November 2021*
Accepted: *07 January 2022*
Published: *15 February 2022*

Citation:
Zhang J, Zeng H, Wang C and Tang Z (2022) Effect of Al_3Zr Dispersoid on Microstructure and Mechanical Properties of Al-Cu-Li Alloy During Composite Spinning-Extrusion Forming. Front. Mater. 9:822589. doi: 10.3389/fmats.2022.822589

INTRODUCTION

With the improvement in the requirements for lightweight structural materials in the aerospace industry, Al-Cu-Li alloys with excellent comprehensive properties such as low density, high elastic modulus, and high specific strength are considered as ideal materials for the manufacture of space launch vehicles with rib-ring cylinders (Rioja et al., 2012; Ahmed and Wu, 2013; Dursun and Soutis, 2014; Yu et al., 2015; El-Aty et al., 2018; Zhang et al., 2018). At present, composite spinning–extrusion (CSE), which combines the advantages of both spinning and extrusion processes, is considered as a new method for the integral formation of ribbed ring cylinders (Domack and Wangner, 2015; Tayon et al., 2019). However, current research on the integral formation of ribbed cylindrical parts is still in the exploration stages, and most of the relevant reports focus on the optimization of process parameters such as temperature, thinning rate, and feed ratio (Zeng et al., 2020; Luo et al., 2018; Zhan et al., 2016; Zhan et al., 2016; Abd-Eltwab et al., 2017; Lin et al., 2018; Xia et al., 2018; Xia et al., 2019). At present, there is no report on the preparation of ribbed ring cylinders through Al-Cu-Li alloy CSE forming.

The macroscopic properties of the Al-Cu-Li alloy depend on its microstructure. Adjusting the microstructure in the second phase is an important method for improving the properties of Al-Cu-Li alloys (Pu et al., 2020; Araullo-Peter et al., 2014; Li et al., 2016; Zhang et al., 2018; Lin et al., 2018).

TABLE 1 | Chemical composition of Al-Cu-Li alloy (wt%).

Cu	Li	Mg	Ag	Zr	Fe	Zn	Si	Ti	Mn	Al
3.77	1.16	0.46	0.31	0.13	0.082	0.0077	0.06	0.0013	0.0015	Bal

Dispersed Al_3Zr dispersoids can pin dislocations and inhibit recrystallization, which causes the formation of the important precipitate phase, thus improving the properties of the Al-Cu-Li alloy (Robson and Prangnell, 2001; Cassell et al., 2019). Therefore, many scholars have explored ways to regulate the precipitation of Al_3Zr and improve the properties of alloys. For example, compared to the traditional single-stage homogenization method, both double-stage homogenization and ramp heating can improve the distribution of Al_3 (Er, Zr) dispersoids, reduce the width of the precipitation-free zone (PFZ) near the grain boundary, and obtain finer Al_3 (Er, Zr) dispersoids and higher number density and volume fraction (Wu et al., 2017). The precipitation of Al_3Zr dispersoids is based on the interaction between the Zr solute and the dislocation climb after Zr atom diffusion to dislocation. In addition, its fine and continuous distribution can reduce the degree of recrystallization and improve mechanical properties (Tsivoulas and Robson, 2015). A_3Zr dispersoids can effectively reduce the thickness of the coarse-grained layer, inhibit the local PFZ, and improve the properties of the Al-Cu-Li alloy (Wang et al., 2021). At present, there is no public report on the formation of Al_3Zr dispersoids and CSE, and its coupling factors and mechanism still need to be further explored. Therefore, it is of great significance to investigate the effect of Al_3Zr dispersion on the microstructure and mechanical properties of CSE ring cylinders.

In this study, blanks with different initial structures were prepared by different heat treatment processes and then subjected to the same CSE forming process. The effects of Al_3Zr dispersoids on the rheological, structural, and mechanical properties of the CSE-formed Al-Cu-Li alloy were investigated using multi-scale observation methods such as optical microscopy (OM), scanning electron microscope (SEM), electron backscatter diffraction (EBSD) analysis, and transmission electron microscopy (TEM). The effects of the dispersed Al_3Zr dispersoids on the microstructure of the CSE-formed coarse-grained layer and the mechanical properties of the CSE-formed alloy were investigated.

MATERIALS AND EXPERIMENTS

Material

The material used in this experiment is an as-cast Al-Cu-Li alloy with a size of φ 480 × 256 mm. The composition of the alloys is summarized in **Table 1**. After free forging, the material was cut into φ 200 mm × 20 mm samples, which were formed by the same CSE forming process after being subjected to three different heat treatment processes. The free forging process conditions were as follows: 440°C, upsetting to φ 650 × 130 mm + three-way forging to 500 × 500 × 120 mm + along the width and length by pulling to 80 × 700 × 700 mm (each pulled down by 20 mm).

Heat Treatment and Composite Spinning–Extrusion Forming

The samples were heat-treated at 510°C for 2 h, 510°C for 4 h, and to 510°C at a rate of 0.85°C/min for 12 h and labeled as #1, #2 and #3, respectively. After heat treatment, the samples were subjected to annealing at 510°C for 2 h and T83 process (T83, 510°C/1 h solution treatment +3% pre-stretching +160°C/27 h). The microstructure of the billet produced by CSE forming is shown in **Figure 1**. The grain structure and coarse second phase types of the three samples before forming were the same, with an average grain size of 156.25 μm. The coarse second phase dispersoids have only the insoluble Al_7Cu_2Fe (arrow in **Figure 1**). The microstructure of the three samples differed only in the amount of precipitated Al_3Zr. There were no Al_3Zr dispersoids in #1, whereas #2 had some Al_3Zr dispersoids, and #3 had a large number of Al_3Zr dispersoids.

CSE forming was carried out on a CNC spinning machine; the size of the billet was φ200 mm × 20 mm, the forming temperature was 300°C, the feed ratio was 1.07 mm/r, and the thinning rate was 82.5%. During CSE forming, the rotating wheel was fed along the axial direction (AD) in a certain track and pressure was applied on the blank, which rotates along the tangential direction (TD) with respect to the core shaft, so that the blank can be plastically deformed to prepare the stiffened barrel shell. A schematic of the forming process is shown in **Figure 2A**. After removing the ends of the CSE-formed ring cylinder, the results are shown in **Figure 2B**. According to the national standard of room-temperature stretching GB/T 228.1–2010, the room-temperature stretched specimen was cut at the thin wall along the middle part of the shell, as shown in **Figure 2D**; the sampling diagram is shown in **Figure 2C**.

Mechanical Properties and Microstructure Characterization

The tensile performance at room temperature was measured using a CSS-44100 tensile tester at a tensile speed of 2 mm/min and an extensometer at 25 mm. Hardness was measured on a CMT-5105 microhardness tester with a load of 500 N and a residence time of 10 s. The metallographic samples were observed using a DSX500 optical microscope. The EBSD samples were electropolished at 15 V for 15 s in a solution of 30% nitric acid and 70% methanol. After removing the stress layer, they were observed using a Zeiss Evo MA10 scanning electron microscope equipped with an EBSD probe. The sample for TEM was mechanically thinned to ~90 μm and then washed into a 3 mm diameter wafer. The electrolysis double injection was performed with a mixture of 30% nitric acid and 70% methanol. The instrument temperature was controlled at −30°C, and an FEI Titan F20 G2 transmission electron

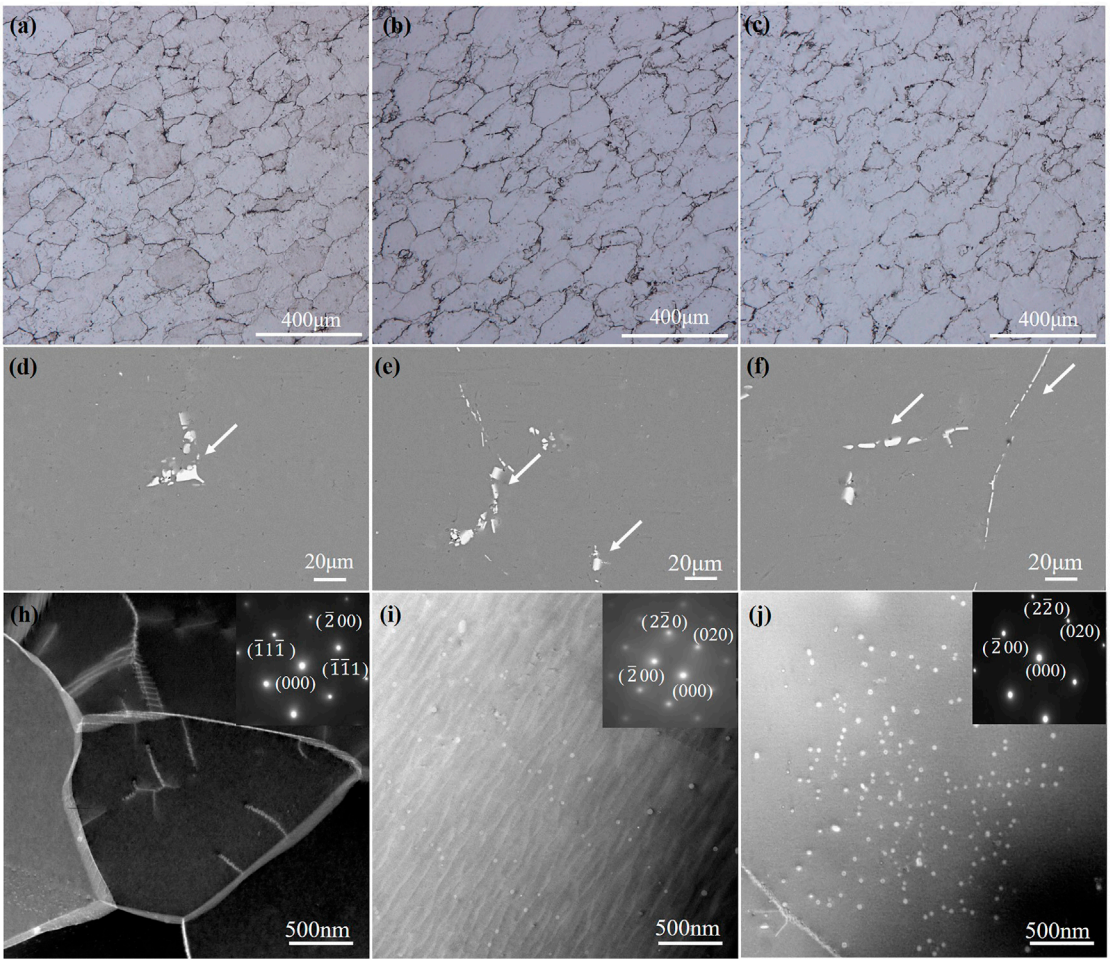

FIGURE 1 | Microstructure of CSE forming blank. **(A,D,H)** 1#, **(B,E,I)** 2#, **(C,F,J)** 3#.

microscope was used for observation under 200 kV operating voltage.

RESULTS AND DISCUSSION

CSE Forming Integrity and Grain Structure

Figures 3A–C show the physical pictures of #1–# 3 after CSE formation. It can be seen that #1 and #2 have different degrees of cracking at the open end, with #1 having the largest degree. Compared with #1 and #2, #3 was formed completely and possessed the optimal forming quality. This indicates that Al_3Zr dispersoids can effectively improve the cracking of CSE-formed shells and promote the overall formation of ring cylinders.

Figures 4A–C shows the EBSD results for #1–#3 with respect to the section of the tube wall after CSE formation (sampling location is shown in **Figure 2C**), wherein the white lines represent low-angle grain boundaries (LAGBs) defined as 2°–15°, and the black lines represent high-angle grain boundaries (HAGBs) defined as >15°. It can be seen that the grains after CSE formation are obviously refined and mainly deformed grains, which are distributed in strips along the circumference of the cylinder wall. The average grain sizes of #1, #2, and #3 are 9.5, 8.9, and 8.1 μm, respectively, as calculated using the Channel software. The grain of #3 was found to be refined as its size decreased from 156.25 to 8.1 μm, which is the largest decrease. **Figures 5A–C** show the HAGBs of #1, #2, and #3, which were 62.4, 53.5, and 48.6%, respectively. This is attributed to the obvious dynamic recrystallization during CSE formation. As CSE formation takes shape, enough energy accumulates in the newly generated recrystallized grains for repeated dynamic recrystallization, resulting in the formation of fine recrystallized grains. At the same time, Al_3Zr has the effect of pinning grain boundaries (Robson and Prangnell, 2001), which can inhibit grain growth to a certain extent. Therefore, after the blank is formed by CSE, the grain is significantly refined.

Mechanical Property

Figure 6 shows the mechanical properties of the #1–#3 following their CSE formation after annealing and T83 treatment. **Figure 6A** shows the stress–strain curves of the three

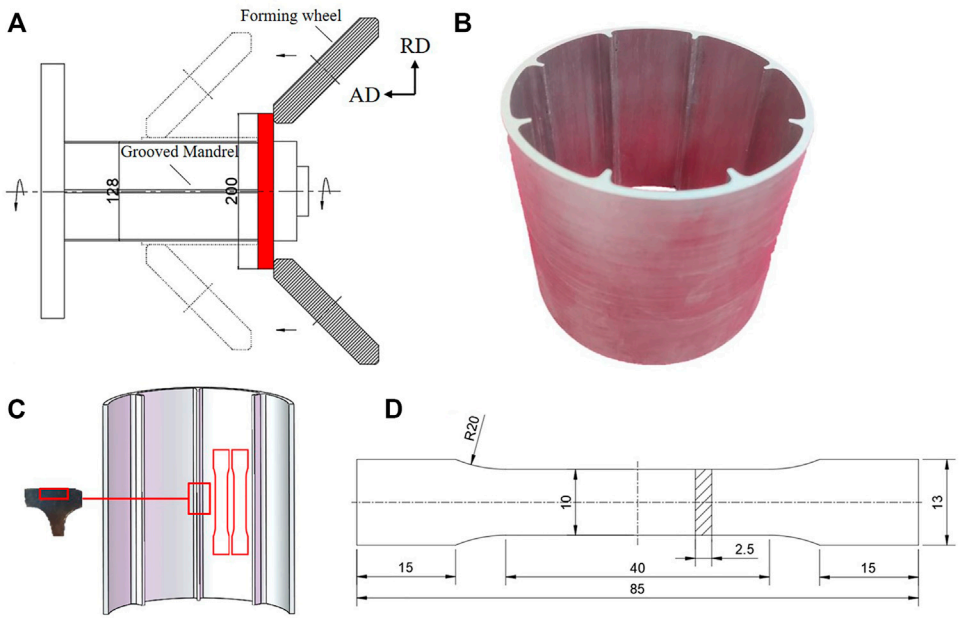

FIGURE 2 | CSE forming schematic diagram and tensile specimen size at room temperature. **(A)** CSE forming schematic, **(B)** CSE forming result, **(C)** Sampling location, **(D)** Tensile dimension at room temperature.

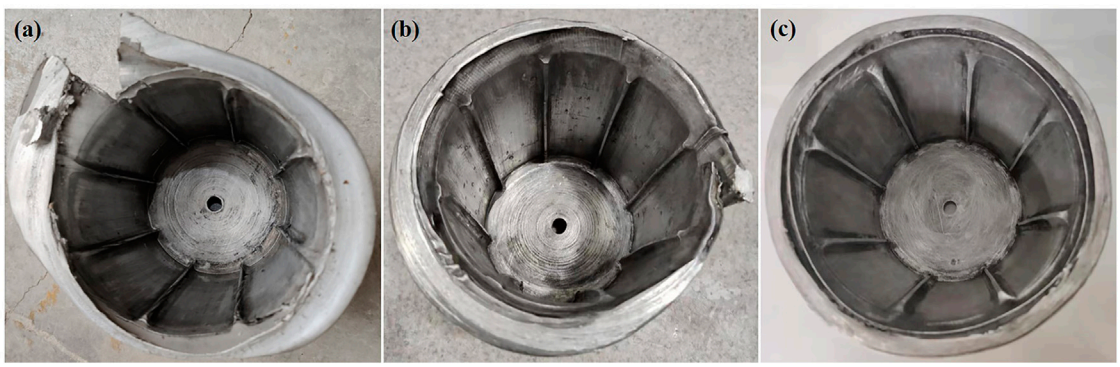

FIGURE 3 | CSE forming results. **(A)**1#, **(B)**2#, **(C)**3#.

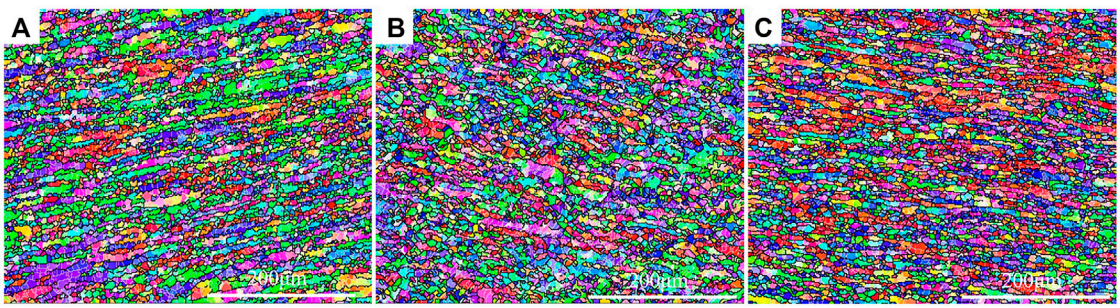

FIGURE 4 | EBSD diagram of sample after CSE forming. **(A)**1#, **(B)**2#, **(C)**3#.

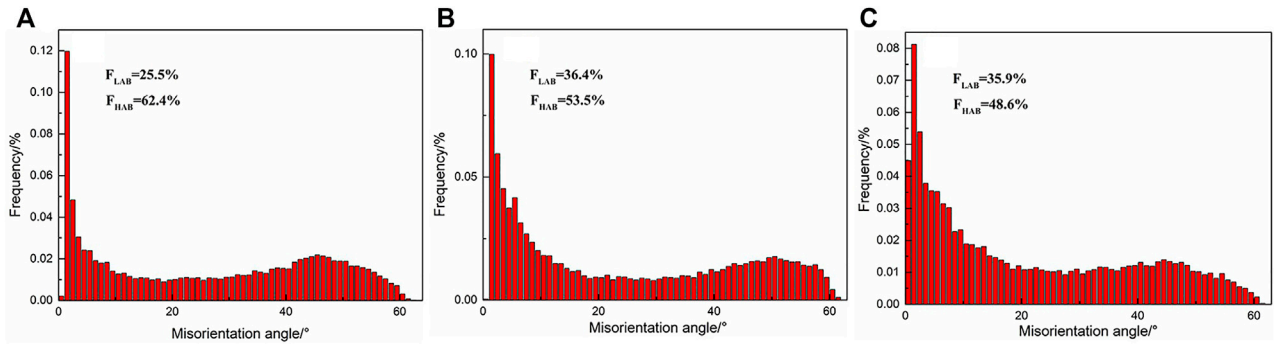

FIGURE 5 | Misorientation distribution maps and volume fraction of LAGBs and HAGBs. **(A)**1#, **(B)**2#, **(C)**3#.

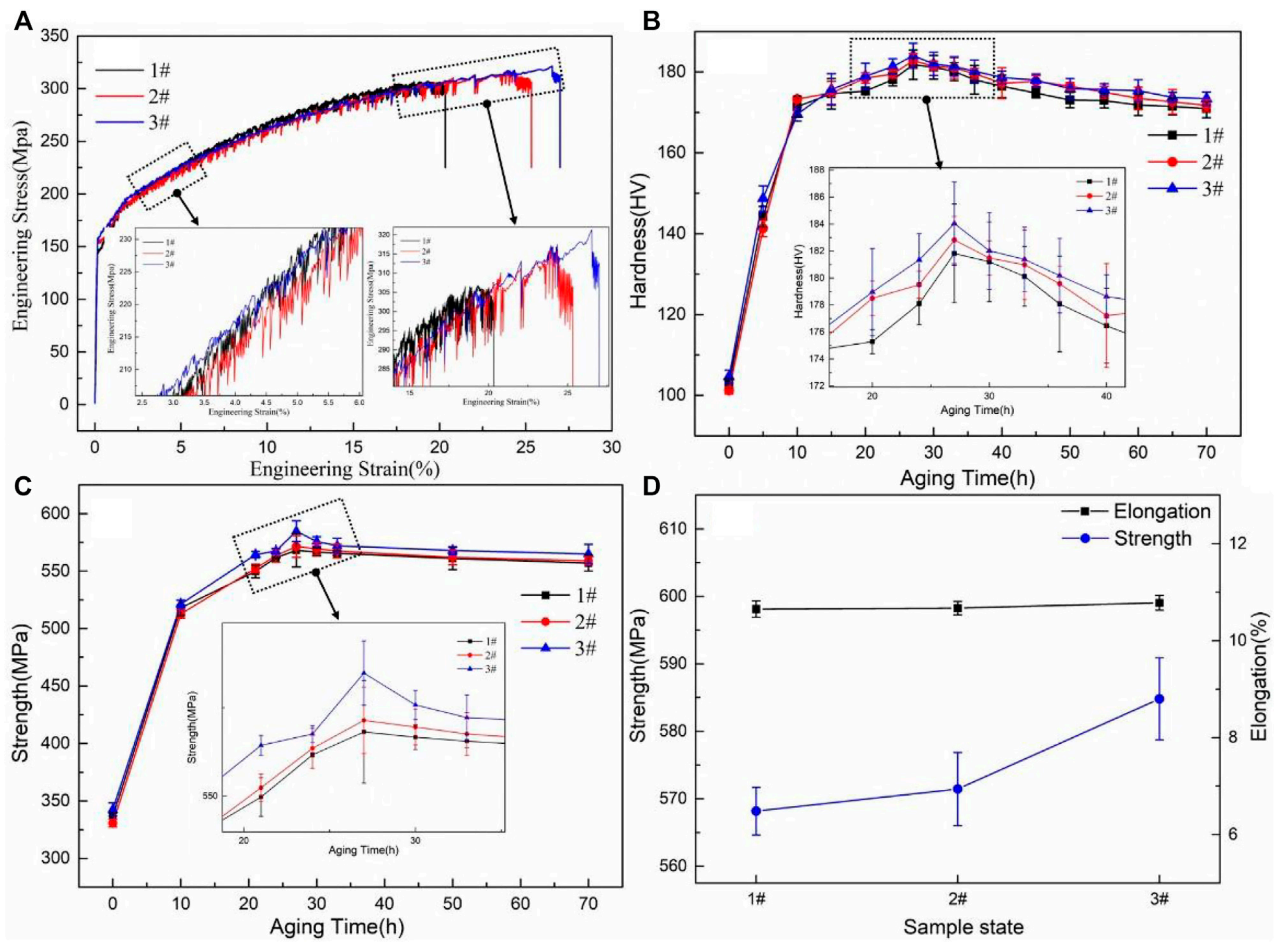

FIGURE 6 | Mechanical properties of specimens after annealing and at T83. **(A)** stress—strain curves of specimens after annealing, **(B)** age hardening curve, **(C)** aging strength curve, **(D)** Mechanical properties of sample at T83 after removing coarse-grained layer.

specimens after annealing at 510°C for 2 h; **Figures 6B–D** shows the age versus hardening curve, age versus strength curve, and T83 state mechanical properties under the T83 process. As shown in **Figure 6A**, the strengths of the three samples after annealing were similar, but the elongation showed a significant difference. The average elongation of #1 is only 20.3%, while those of #2 and #3 were 25.3 and 27.1%, respectively. The elongation of #3 increased by 33.5% compared to that of #1, indicating that the dispersed Al_3Zr

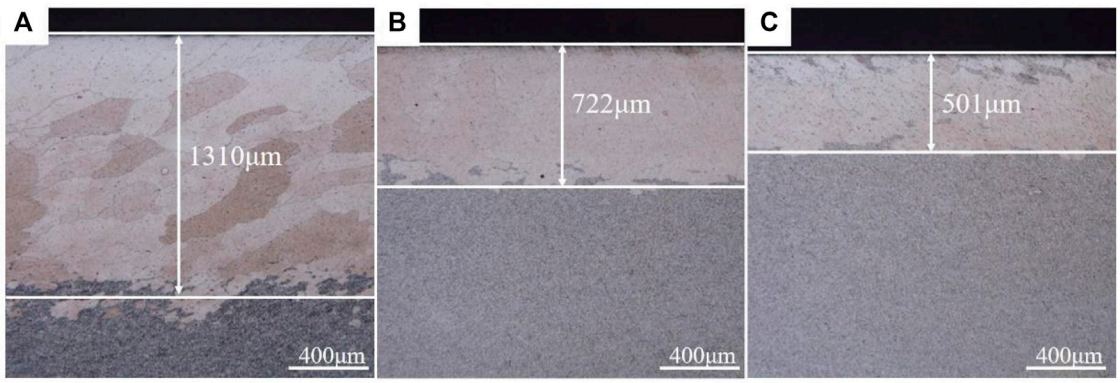

FIGURE 7 | OM diagram of the sample after annealing. **(A)**1#, **(B)**2#, **(C)**3#.

dispersoids can effectively improve the ductility of the material. As shown in **Figures 6B,C**, the peak aging time of #1–#3 in the T83 process is 27 h, and the corresponding hardness values are 181.82, 182.82, and 183.04 Hv, and the peak strengths are 568, 571, and 584 MPa. As shown in **Figure 6D**, there is no significant difference in the elongation among #1–#3 after removing the coarse-grained layer. Also, the average tensile strength increases with the precipitation of Al_3Zr dispersoids, indicating that the precipitation of Al_3Zr dispersoids is conducive to the improvement of the mechanical properties of the Al-Cu-Li alloy.

Microstructure

OM Observation

Figures 7A–C show the OM images of #1–#3 annealed at 510°C for 2 h after CSE formation. **Figure 7** shows that the central layer of the three samples had a fine grain structure, and the surface of the coarse-grained layer was thick. The thickness of the coarse-grained layer was 1,310 μm for #1, 722 μm for #2, and 501 μm for #3. In general, during CSE formation, the spinning wheel acts directly on the surface layer of the sample in the form of applying point-by-point pressure, so that the deformation of the surface layer is larger than that of the central layer. This results in high deformation and storage of surface grains, and a coarse-grained layer is easily formed after annealing at high temperatures. Unlike to the fine grain structure in the central layer, the coarse grains in the surface layer tend to crack first during the tensile process, resulting in low ductility of the material. This explains the low elongation of #1 (as shown in **Figure 6A**). Compared with sample 1#, the coarse-grained thickness of sample 3# decreased from 1,310 to 501 μm, and the corresponding elongation increased from 20.3 to 27.1%. This is attributed to Al_3Zr pinning grain boundaries and inhibiting the growth of surface grains during static recrystallization. The effect of Al_3Zr on reducing the coarse-grain layer thickness of Al-Cu-Li alloy has also been confirmed in another study on rolled plate by our research group (Wang et al., 2021).

TEM Observation

The strengthening mechanism of the Al-Cu-Li alloy follows solid solution strengthening, fine grain strengthening, second-phase particle strengthening, and deformation strengthening (Dorin et al., 2018). Owing to the same chemical composition, spinning process, and solution system of the three samples, the strength difference mainly comes from the refinement of the grains and the precipitation of the second-phase dispersoids. In A-Cu-Li alloys, the main contribution to strengthening is the precipitation of T_1 phase (Decreus., et al 2013; Dorin., et al 2014). **Figures 8A–C** show the STEM diagram observed along the <110> Al direction of the cylinder wall of #1–#3; **Figure 9A,B** show the results of the mass statistics of the average size and the number of the strengthening phases at a unified scale. As shown in **Figures 9A,B**, compared to #1 (100.3 nm) and #2 (91.8 nm), the average length of the T_1 phase (77.5 nm) for #3 was the smallest, indicating that #3 had the highest quantitative density; its corresponding tensile strength was also the highest (as shown in **Figure 3D**). This indicates that the dispersed Al_3Zr can promote the precipitation of the T_1 phase and refine the size of the grains, thereby improving the strength of the material.

CONCLUSION

In summary, the effects of Al_3Zr dispersoids on the microstructure and mechanical properties of CSE ring cylinder of Al-Cu-Li alloy were studied by SEM, TEM, EBSD and mechanical test, and the promoting effect of Al_3Zr dispersoids on CSE ring cylinder was revealed. On the basis of the study herein, main conclusions were drawn as follows:

1) By regulating the dispersion phase of Al_3Zr, the cracking of the ring cylinder can be effectively suppressed, the thickness of the coarse-grained layer can be significantly reduced, and the elongation of the ring cylinder can be improved. When the Al_3Zr dispersoids precipitated in large numbers, the coarse-grained layer decreased from 1,310 μm to 501 μm, and the corresponding elongation increased from 20.3 to 27.1%.

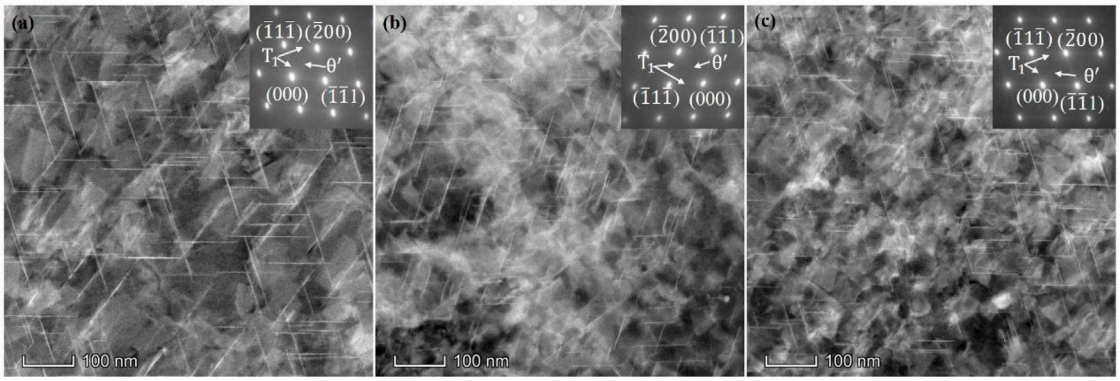

FIGURE 8 | STEM diagram taken along <110 > Al direction of the sample at T83. **(A)**1#, **(B)**2#, **(C)**3#.

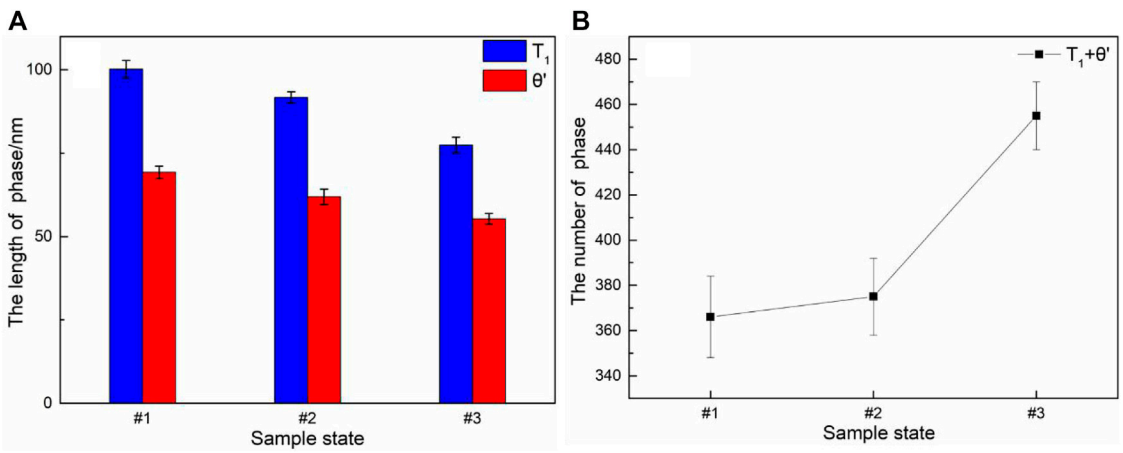

FIGURE 9 | Length and quantity relation of T_1 and θ′ phases. **(A)** average length, **(B)** quantity.

2) The microstructure and strength properties of the CSE ring cylinder were affected by the different dispersion particle distributions in the blank. With an increase in the amount of precipitated Al_3Zr in the initial billet, the average grain size of the forming parts gradually decreased, and the density of the T_1 phase significantly increased, thereby improving the strength performance of the forming ring cylinder. The average length of the T_1 phase was reduced from 100.3 to 77.5 nm, the tensile strength increased by 16 MPa, and the yield strength is increased by 20 MPa.

DATA AVAILABILITY STATEMENT

The original contributions presented in the study are included in the article/Supplementary Material, further inquiries can be directed to the corresponding author.

AUTHOR CONTRIBUTIONS

JZ: Conceptualization, Methodology, Software, Data curation, and Writing— original draft. CW: Writing—review and editing, Conceptualization, Methodology, and Software. HZ: Conceptualization, Methodology, Software, and Supervision. ZT: Supervision. All authors have read and agreed to the published version of the manuscript.

FUNDING

The authors gratefully acknowledge financial supports from the National Key R and D Program of China (Grant No. 2020YFA0711104), National Natural Science Foundation of China (Grant No. U21B6004) and Major Project of Scientific Innovation of Hunan Province(Grant No. 2021GK1040).

REFERENCES

Abd-Eltwab, A. A., El-Abden, S. Z., Ahmed, K. I. E., El-Sheikh, M. N., and Abdel-Magied, R. K. (2017). An Investigation into Forming Internally-Spline Sleeves by ball Spinning. *Int. J. Mech. Sci.* 134, 399–410. doi:10.1016/j.ijmecsci.2017.10.033

Ahmed, B., and Wu, S. J. (2013). Aluminum Lithium Alloys (Al-Li-Cu-X)-New Generation Material for Aerospace Applications. *Amm* 440, 104–111. doi:10.4028/www.scientific.net/amm.440.104

Araullo-Peters, V., Gault, B., Geuser, F. D., Deschamps, A., and Cairney, J. M. (2014). Microstructural Evolution during Ageing of Al-Cu-Li-X Alloys. *Acta Materialia* 66, 199–208. doi:10.1016/j.actamat.2013.12.001

Cassell, A. M., Robson, J. D., Race, C. P., Eggeman, A., Hashimoto, T., and Besel, M. (2019). Dispersoid Composition in Zirconium Containing Al-Zn-Mg-Cu (AA7010) Aluminium alloy. *Acta Materialia* 169, 135–146. doi:10.1016/j.actamat.2019.02.047

Decreus, B., Deschamps, A., De Geuser, F., Donnadieu, P., Sigli, C., and Weyland, M. (2013). The Influence of Cu/Li Ratio on Precipitation in Al-Cu-Li-X Alloys. *Acta Materialia* 61 (6), 2207–2218. doi:10.1016/j.actamat.2012.12.041

Domack, M. S., and Wagner, J. A. (2015). Innovative Manufacturing of Cylinders with Integral Stiffeners. *Natl. Aeronautics Space Adm.*. Available at: https://ntrs.nasa.gov/citations/20150006865.

Dorin, T., De Geuser, F., Lefebvre, W., Sigli, C., and Deschamps, A. (2014). Strengthening Mechanisms of T1 Precipitates and Their Influence on the Plasticity of an Al-Cu-Li alloy. *Mater. Sci. Eng. A* 605, 119–126. doi:10.1016/j.msea.2014.03.024

Dorin, T., Vahid, A., and Lamb, J. (2018). Aluminium Lithium Alloys. *J. Mater. Sci.* 22 (5), 387–438. doi:10.1016/B978-0-08-102063-0.00011-4

Dursun, T., and Soutis, C. (2014). Recent Developments in Advanced Aircraft Aluminium Alloys. *Mater. Des. (1980-2015)* 56, 862–871. doi:10.1016/j.matdes.2013.12.002

El-Aty, A., Xu, Y., Guo, X., Zhang, S.-H., Ma, Y., and Chen, D. (2018). Strengthening Mechanisms, Deformation Behavior, and Anisotropic Mechanical Properties of Al-Li Alloys: A Review. *J. Adv. Res.* 10 (C), 49–67. doi:10.1016/j.jare.2017.12.004

Li, H., Huang, D., Kang, W., Liu, J., Ou, Y., and Li, D. (2016). Effect of Different Aging Processes on the Microstructure and Mechanical Properties of a Novel Al-Cu-Li Alloy. *J. Mater. Sci. Technol.* 32, 1049–1053. doi:10.1016/j.jmst.2016.01.018

Lin, Y., Lu, C., Wei, C., and Zheng, Z. (2018). Effect of Aging Treatment on Microstructures, Tensile Properties and Intergranular Corrosion Behavior of Al-Cu-Li alloy. *Mater. Characterization* 141, 163–168. doi:10.1016/j.matchar.2018.04.043

Luo, W., Chen, F., Xu, B., Yang, Z., Guo, Y., Lu, B., et al. (2018). Study on Compound Spinning Technology of Large Thin-Walled Parts with Ring Inner Ribs and Curvilinear Generatrix. *Int. J. Adv. Manuf Technol.* 98, 1199–1216. doi:10.1007/s00170-018-2334-x

Pu, Q., Jia, Z., Kong, Y., Yang, Q., Zhang, Z., Fan, X., et al. (2020). Microstructure and Mechanical Properties of 2195 Alloys Prepared by Traditional Casting and spray Forming. *Mater. Sci. Eng. A* 784, 139337. doi:10.1016/j.msea.2020.139337

Rioja, R. J., Liu, J., and Roberto, J. (2012). The Evolution of Al-Li Base Products for Aerospace and Space Applications. *Metall. Mat Trans. A.* 43 (9), 3325–3337. doi:10.1007/s11661-012-1155-z

Robson, J. D., and Prangnell, P. B. (2001). Dispersoid Precipitation and Process Modelling in Zirconium Containing Commercial Aluminium Alloys. *Acta Materialia* 49 (4), 599–613. doi:10.1016/S1359-6454(00)00351-7

Robson, J. D., and Prangnell, P. B. (2003). Modelling Al_3Zr Dispersoid Precipitation in Multicomponent Aluminium Alloys. *Mater. Sci. Eng. A.* 352, 240–250. doi:10.1016/S0921-5093(02)00894-8

Tayon, W. A., Domack, M. S., and Wagner, J. A. (2019). Characterization of 10-ft. Diameter Aluminum Alloy 2219 Integrally Stiffened Cylinders. Available at: https://www.researchgate.net/publication/332802954_Characterization_of_10-ft_Diameter_Aluminum_Alloy_2219_Integrally_Stiffened_Cylinders.

Tsivoulas, D., and Robson, J. D. (2015). Heterogeneous Zr Solute Segregation and Al3Zr Dispersoid Distributions in Al-Cu-Li Alloys. *Acta Materialia* 93, 73–86. doi:10.1016/j.actamat.2015.03.057

Wang, C., Zhang, J., Yi, Y., and Zhu, C. (2021). Effect of Pretreatment and Cryogenic Temperatures on Mechanical Properties and Microstructure of Al-Cu-Li Alloy. *Materials* 14, 4873. doi:10.3390/ma14174873

Wu, H., Wen, S. P., Huang, H., Li, B. L., Wu, X. L., Gao, K. Y., et al. (2017). Effects of Homogenization on Precipitation of Al 3 (Er,Zr) Particles and Recrystallization Behavior in a New Type Al-Zn-Mg-Er-Zr alloy. *Mater. Sci. Eng. A* 689 (17), 313–322. doi:10.1016/j.msea.2017.02.071

Xia, Q.-X., Long, J.-C., Zhu, N.-Y., and Xiao, G.-F. (2019). Research on the Microstructure Evolution of Ni-Based Superalloy Cylindrical Parts during Hot Power Spinning. *Adv. Manuf.* 7, 52–63. doi:10.1007/s40436-018-0242-9

Xiao, G., Zhu, N., Long, J., Xia, Q., and Chen, W. (2018). Research on Precise Control of Microstructure and Mechanical Properties of Ni-Based Superalloy Cylindrical Parts during Hot Backward Flow Spinning. *J. Manufacturing Process.* 34 (AUG), 140–147. doi:10.1016/j.jmapro.2018.05.034

Yu, N., Shang, J., Cao, Y., Ma, D., and Liu, Q. (2015). Comparative Analysis of Al-Li Alloy and Aluminum Honeycomb Panel for Aerospace Application by Structural Optimization. *Math. Probl. Eng.* 2015, 1–12. doi:10.1155/2015/815257

Zeng, X., Fan, X. G., Li, H. W., Zhan, M., Li, S. H., Wu, K. Q., et al. (2020). Heterogeneous Microstructure and Mechanical Property of Thin-Walled Tubular Part with Cross Inner Ribs Produced by Flow Forming. *Mater. Sci. Eng. A* 790, 139702. doi:10.1016/j.msea.2020.139702

Zhan, M., Wang, X., and Long, H. (2016). Mechanism of Grain Refinement of Aluminium alloy in Shear Spinning under Different Deviation Ratios. *Mater. Des.* 108, 207–216. doi:10.1016/j.matdes.2016.06.095

Zhang, X., Chen, Y., and Hu, J. (2018). Recent Advances in the Development of Aerospace Materials. *Prog. Aerospace Sci.* 97 (FEB.), 22–34. doi:10.1016/j.paerosci.2018.01.001

Conflict of Interest: The authors declare that the research was conducted in the absence of any commercial or financial relationships that could be construed as a potential conflict of interest.